Autonomous Robots 13, 73–86, 2002
© 2002 Kluwer Academic Publishers. Manufactured in The Netherlands.

Relating Torque and Slip in an Odometric Model for an Autonomous Agricultural Vehicle

D.R. LINDGREN
Department of Engineering Science, University of Oxford, UK; Silsoe Research Institute, Silsoe, UK

T. HAGUE
Silsoe Research Institute, Silsoe, UK

P.J. PROBERT SMITH
Department of Engineering Science, University of Oxford, UK

J.A. MARCHANT
Silsoe Research Institute, Silsoe, UK

Abstract. This paper describes a method of considering the slip that is experienced by the wheels of an agricultural autonomous guided vehicle such that the accuracy of dead-reckoning navigation may be improved. Traction models for off-road locomotion are reviewed. Using experimental data from an agricultural AGV, a simplified form suitable for vehicle navigation is derived. This simplified model relates measurements of the torques applied to the wheels with wheel slip, and is used as the basis of an observation model for odometric sensor data in the vehicle's extended Kalman filter (EKF) navigation system. The slip model parameters are included as states in the vehicle EKF so that the vehicle may adapt to changing surface properties. Results using real field data and a simulation of the vehicle EKF show that positional accuracy can be increased by a slip-aware odometric model, and that when used as part of a multi-sensor navigation system, the consistency of the EKF state estimator is improved.

Keywords: navigation, Kalman filter, odometry, slip, traction

1. Introduction

Autonomous outdoor vehicles for agriculture have been investigated for some time; a recent collection of work in the area can be found in Jahns (2000). The problem of determining position with adequate precision and reliability has yet to be completely solved, although GPS for general position within a field, and machine vision for fine positioning relative to crop rows, are emerging as the most promising exterioceptive sensors.

Although receiving less attention, odometers are probably the most widely used navigation sensors. Odometry is simple and low cost, and can provide information when there are no visible features for vision sensors, and near boundaries, or close to hedges and trees where shadowing is a problem for GPS (circumstances which often occur together). Odometry can also provide a means of interpolation between infrequent GPS position fixes. The disadvantage is susceptibility to errors from a variety of sources, including wheel slip. These errors are cumulative, giving a rapid loss in positional accuracy.

The most obvious approach to reducing these errors is to take odometric measurements from unpowered wheels. There are a number of complications with this approach. Firstly, the mechanical constraints; the odometry wheels must be of large diameter to avoid surface roughness affecting the measured distance. The

wheels must be pressed into intimate contact with the ground at all times, and on a soil surface, the wheels must be designed to avoid accumulated dirt which would also affect the measured distance. Finally, if the wheels are not to be castored, the axis of the odometric wheels must be collinear with that of the driven wheels. These criteria are ideally met by the driven wheels themselves. The second factor to be considered is the ability to control the vehicle should wheel slip occur. If odometric measurement is taken from separate wheels only, when slippage of the driven wheels occurs it becomes impossible to measure (and hence control) the speed of rotation of the driven wheels. Should the vehicle control system respond to the reduced vehicle speed by increasing the torque applied to the driven wheels, gross wheel spin is likely to result.

An alternative approach is to consider the slip experienced by the driven wheels within an odometric model. Various measures have been devised to reduce, or compensate for, systematic odometric errors in laboratory robot vehicles (Borenstein, 1996). It is important to realize that the physical processes involved in wheel slip are different for vehicles on a soil surface. Agricultural soil is generally not smooth and flat and the soil itself deforms as the wheels pass over it applying a horizontal (in the plane of the soil) force to it. In these cases, not all wheel motion translates to a motion of the vehicle with respect to the environment coordinate frame; some of the wheel motion contributes to soil deformation. This corresponds to wheel slip. Moreover, it may be undesirable or impossible to eliminate slip; maximum traction occurs at non-zero values of slip.

An approach to off-road slip modeling at the Australian Centre for Field Robotics (Le et al., 1997; Scheding et al., 1997) uses the trajectory of the vehicle as measured by a combination of sensors to estimate slip angle (i.e., the angle between the orientation of the vehicle body and the velocity vector) which is non-zero in the presence of *lateral* slip. In contrast we wish to model wheel slip in the *longitudinal* direction, arising from torques acting on the wheels. Longitudinal slip is defined by,

$$s = 1 - \frac{v_a}{v_m} \tag{1}$$

where v_a and v_m are the actual and odometrically measured translational speeds of the centre of the wheel.

The work of Bekker (Bekker, 1960, 1962) provides the basis for a number of works on modeling of slip. Using an experimental rig to measure the deformation of soil for varying values of applied shear force, Bekker was able to construct plots of the relationship between shear force and slip for each of these soils. He modeled the observed soil shear/deformation relationship using curves having the form of an over-damped sinusoid.

Using experimental data for typical off-road soils, Janosi and Hanamoto (1961) proposed that Bekker's quite complex model was difficult to use in practice for most normal soils, and suggested instead that the shear stress ϱ and deformation j may be related by the simplified model:

$$\varrho = \varrho_{max}(1 - e^{-\frac{j}{K}}) \tag{2}$$

where parameter K depends upon soil properties and ϱ_{max} is given by the Mohr-Coulomb equation (Smith, 1982; Craig, 1992) for maximum soil shear strength

$$\varrho_{max} = c + \sigma \tan\phi \tag{3}$$

given soil properties c and ϕ, and normal stress σ.

Though much of the previous work on slip modeling relates to tracked vehicles, Okello et al. (1994) found that a model derived from that of Janosi and Hanamoto gave a good fit to experimental data for both wheels and tracks. In the rest of this paper, we consider the application of these findings in the development of a slip-aware observation model for interpretation of odometric data from the driven wheels of an agricultural AGV.

2. Experimental Vehicle

2.1. Description

The platform used is an experimental autonomous agricultural vehicle (Fig. 1) designed for plant scale treatment of crops (Hague and Tillett, 1996). The vehicle spans one 2 m wide bed of crop plants. Automatic control of a spray application, guided by a vision system, allows the vehicle to identify and chemically treat individual plants rather than the entire plot. While this has significant environmental advantages, it would be unrealistic and uneconomic for the task to be completed manually.

The vehicle is powered by a petrol engine, which drives each of the two front wheels via independent hydrostatic transmissions giving control of vehicle speed and steering. The hydrostatic units are electrically actuated, and control is achieved by two methods. When the engine is not running, PID control is used to position the hydrostatic pumps into the neutral position; PD

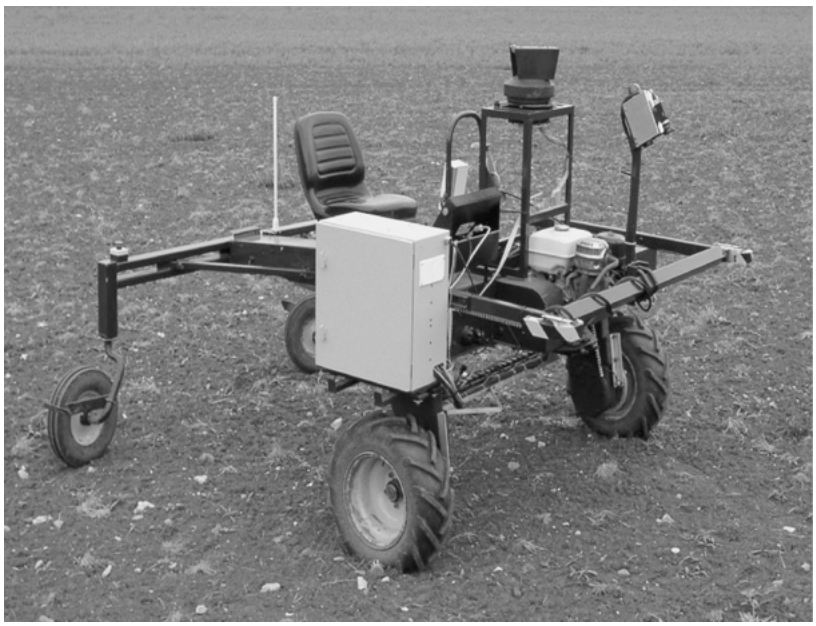

Figure 1. The experimental vehicle, with laser scanner fitted.

control of the angular velocity of each wheel is applied when the engine is started.

2.2. *Sensing Systems*

The vehicle is equipped with odometers, in the form of an incremental encoder fitted to each of the driven wheels, to provide wheel motion feedback. In order to investigate and exploit the torque/slip relationship, a method of torque measurement is also needed for each of the driven wheels. A purpose built vehicle could use a range of convenient and inexpensive measurement methods, for example, sensing the pressure applied to hydraulic drive motors or the current through electric drives. For experimental purposes the existing vehicle was equipped for torque measurement using sensors which could be interposed between the wheels and their hubs.

A sensor design which separates vertical loading from the rotational torque was adopted because the forces due to the vehicle's weight are quite significant in comparison to those arising from wheel torque. It consists of two circular metal plates of diameter 240 mm connected through an axis perpendicular to the plane of the discs and through their centres by a shaft and roller bearing such that the disks would be free to rotate relative to each other about that axis. The shaft supports the weight of the vehicle so that vertical loading has no effect on the torque sensor reading. The two plates are also connected by a load cell (mounted parallel to, and between the plates) which stops the plates' rotation relative to one another, and gives a force reading when torque, about the plates' central axis, is applied. One plate bolts to the original wheel mounting on the vehicle, and the other to the wheel itself. Since the whole assembly rotates with the wheel during operation, output from the load cell is communicated to the vehicle computer by radio telemetry. The torque sensors were calibrated before installation on the vehicle by adjusting the gain of the preamplifiers to give matched readings for an applied torque of 100 Nm; although as will be seen later, the on-line estimation of the slip model parameters obviates the need for precise calibration.

Tests on slip require accurate knowledge of the vehicle's motion to compare with the odometric estimate. This is provided by a combination of laser and inertial sensors. Two accelerometers give the vehicle's forward and lateral accelerations, and two gyroscopic sensors of the vibrating structure type are used to provide the vehicle's yaw and pitch rates. 'Ground truth' is provided by a laser scanner, which measures bearing to a number of external retro-reflective beacons. The scanner allows a high accuracy estimate of the vehicle position to be obtained. However, accurately surveyed external beacons are required, and the system is only suited to sites

which are reasonably level. Thus it is not suitable for use on a vehicle in general environments, but is adequate for experimental studies.

2.3. Path Formulation

Commanded paths for the vehicle may be composed of multiple segments, which may each take the form of a straight line, circular arc or quadratic spline. The segments are specified by the cartesian coordinates of their end points plus an additional control point where necessary, and the initial and final speeds. Where the speeds differ, a constant acceleration is used.

2.4. Kalman Filter Navigation

The vehicle uses an Extended Kalman Filter (EKF) to fuse sensor data and calculate position and orientation as it moves. The vehicle's EKF assumes that the process may be described by the general non-linear state transition equation,

$$\mathbf{x}(k+1) = \mathbf{f}(\mathbf{x}(k), \mathbf{u}(k), k) + \mathbf{v}(k) \tag{4}$$

and may be observed by the non-linear sensor model,

$$\mathbf{z}(k) = \mathbf{h}(\mathbf{x}(k)) + \mathbf{w}(k). \tag{5}$$

where at time k, $\mathbf{x}(k)$ is the state, $\mathbf{u}(k)$ is an input vector, $\mathbf{z}(k)$ is the observation vector and $\mathbf{v}(k)$ and $\mathbf{w}(k)$ are the zero mean process and observation noise respectively.

Following the notation of Bar-Shalom and Fortmann (1988), the first order extended Kalman filter state estimator for this system makes the prediction $\hat{\mathbf{x}}(k+1 \mid k)$ of state $\mathbf{x}(k+1)$ using Eq. (4)

$$\hat{\mathbf{x}}(k+1 \mid k) = \mathbf{f}(\hat{\mathbf{x}}(k \mid k), \mathbf{u}(k), k) \tag{6}$$

with covariance

$$\mathbf{P}(k+1 \mid k) = \mathbf{F}(k)\mathbf{P}(k \mid k)\mathbf{F}'(k) + \mathbf{Q}(k) \tag{7}$$

Where $\mathbf{F}(k) = \frac{\partial \mathbf{f}}{\partial \mathbf{x}} \mid_{\mathbf{x}=\hat{\mathbf{x}}(k|k),\mathbf{u}=\mathbf{u}(k)}$, and $\mathbf{Q}(k)$ is the variance of noise input $\mathbf{v}(k)$.

Observations $\mathbf{z}(k+1)$ are then incorporated using Kalman gain $\mathbf{W}(k+1)$ to compute corrected state estimate and its covariance

$$\hat{\mathbf{x}}(k+1 \mid k+1) = \hat{\mathbf{x}}(k+1 \mid k) + \mathbf{W}(k+1)(\mathbf{z}(k+1) - \hat{\mathbf{z}}(k+1 \mid k)) \tag{8}$$

$$\mathbf{P}(k+1 \mid k+1) = \mathbf{P}(k+1 \mid k) - \mathbf{W}(k+1)\mathbf{S}(k+1) \times \mathbf{W}'(k+1) \tag{9}$$

where

$$\mathbf{W}(k+1) = \mathbf{P}(k+1 \mid k)\mathbf{H}'(k+1)\mathbf{S}^{-1}(k+1) \tag{10}$$

$$\mathbf{S}(k+1) = \mathbf{H}(k+1)\mathbf{P}(k+1 \mid k)\mathbf{H}'(k+1) + \mathbf{R}(k+1) \tag{11}$$

Here $\hat{\mathbf{z}}(k+1 \mid k) = \mathbf{h}(\hat{\mathbf{x}}(k+1 \mid k))$, $\mathbf{H}(k+1) = \frac{\partial \mathbf{h}}{\partial \mathbf{x}}|_{\mathbf{x}=\hat{\mathbf{x}}(k+1|k)}$, and $\mathbf{R}(k+1)$ is the covariance of observation noise $\mathbf{w}(k+1)$.

For the vehicle considered here, a nine element state takes the following form:

$$\mathbf{x}(k) = [x \; y \; \theta \; v \; \Omega \; \dot{v} \; \dot{\Omega} \; \alpha_1 \; \alpha_2]' \tag{12}$$

where, at time k:

x is the x-coordinate position of the vehicle with respect to the world coordinate frame;
y is the y-coordinate position of the vehicle;
θ is the bearing of the vehicle measured anti-clockwise from the $y = 0$ axis;
v is the vehicle's linear speed;
Ω is the angular speed or yaw rate;
$\dot{v}$ is the linear acceleration;
$\dot{\Omega}$ is the angular acceleration;
α_1 is the pitch inclination angle;
α_2 is the roll inclination angle.

The process model is derived from that described in Hague et al. (1997); although the original form used a clothoid navigation scheme as opposed to the cartesian system described here, the principles behind the EKF derivation remain identical. The state transition is modeled by:

$$\mathbf{f}(\mathbf{x}, \mathbf{u}) = \begin{bmatrix} x + \tau v \cos\theta \\ y + \tau v \sin\theta \\ \theta + \tau\Omega \\ v + \tau\dot{v} \\ \Omega + \tau\dot{\Omega} \\ \dot{v} \\ \dot{\Omega} \\ \alpha_1 + \tau\dot{\alpha}_1 \\ \alpha_2 + \tau\Omega\alpha_1 \end{bmatrix} \tag{13}$$

Here τ denotes the time period between steps k and $k+1$.

The input vector $\mathbf{u}(k)$ has just one element $\dot{\alpha}_1$, the vehicle pitch rate, which is derived directly from the pitch gyro. Since the vehicle is not equipped to measure roll rate, the prediction of α_2 includes a small angle approximation of the rotation of roll and pitch angles when the vehicle turns around the yaw axis.

The EKF uses measurements from the sensors to update the state estimate. The sensors can be separated into three groups, inertial, odometric, and the exterioceptive laser scanner. The observation noise is assumed to be uncorrelated between the sensors. In practice, this property allows the observations to be processed sequentially rather than at once as a parallel update, with some computational advantage (Willner et al., 1976). This separation also allows data from some sensors to be omitted; this is useful for experimental purposes by allowing post-processing of the recorded sensor data using selected combinations of sensor inputs.

The inertial sensor observations are $\mathbf{z}_{ins}(k) = [a_1\ a_2\ g_1]'$, where a_1 and a_2 are the readings of the forward and lateral accelerometers, g_1 is the yaw gyro reading. The accelerometer readings are expressed in units of g ms^{-2} (g denotes the gravitational acceleration). The observation can be modeled by:

$$\mathbf{h}_{ins}(\mathbf{x}) = \begin{bmatrix} \dot{v}/g + \alpha_1 \\ v\Omega/g - \alpha_2 \\ \Omega \end{bmatrix} \tag{14}$$

Again, small angle approximations have been used for $\alpha_{1,2}$. In practice this is a valid approximation for a wide range of terrain. Observation noise variances of 4.5×10^{-4}, 3.0×10^{-4} and 6.5×10^{-5} respectively were measured for the particular forward and lateral accelerometers and yaw gyroscope used.

The odometers provide the observation $\mathbf{z}_{odo}(k) = [c_1\ c_2]'$ where c_1 and c_2 are respectively the counts of the left and right odometer over time period τ. The original odometric observation model used by Hague et al. (1997) took the form:

$$\mathbf{h}_{odo}(\mathbf{x}) = \begin{bmatrix} \frac{\tau}{\Gamma R_w}\left(v - \frac{W}{2}\Omega\right) \\ \frac{\tau}{\Gamma R_w}\left(v + \frac{W}{2}\Omega\right) \end{bmatrix} \tag{15}$$

Or in a more compact notation:

$$z_{odo} = \frac{\tau}{\Gamma R_w}\left(v \pm \frac{W}{2}\Omega\right) \tag{16}$$

Here W is the lateral separation of vehicle wheels, R_w is the wheel radius and Γ is a scaling between odometric counts and the angle of rotation in radian. The above model does not take account of wheel slip, and odometric errors were assumed to be dominated by quantisation error in the measurement. Given the odometric resolution of 285 counts per radian, a constant odometric variance of 3.1×10^{-6} rad^2 was used.

The laser scanner used to give absolute positioning measures bearing to a number of retroreflective targets placed at known locations; these can be integrated with the vehicle state using the following model:

$$\mathbf{h}_{lz}(\mathbf{x}) = \tan^{-1}\left(\frac{Y_b - y}{X_b - x}\right) - \theta \tag{17}$$

Here (X_b, Y_b) is the known beacon location. Since there are a number of beacons (a minimum of three is necessary for position and orientation to be observable) and they are not uniquely identified, the correspondence problem is solved by selecting the beacon which gives the smallest innovation. Laser scanner observations arrive asynchronously, and are incorporated in the state estimate when received. The scanner performs 3.6 scans per second, and in total 15 beacons were employed, although not all were simultaneously visible. In practice approximately 30 observations were received per second. A constant variance of 1×10^{-4} rad^2 was used for beacon bearing observations.

3. Slip Model Development

3.1. Introduction

A number of models for slip may be found in the literature which assume a dependence on tractive effort; the majority are refined versions of Bekker's original (Bekker, 1960, 1962). Although the exact form varies, we begin with the simple model presented by Okello et al. (1994) relating Coefficient of Traction (C_T) to slip (s):

$$C_T = A\left[1 - \frac{B}{s}(1 - e^{-\frac{s}{B}})\right], \tag{18}$$

where A and B are parameters that determine the shape of the function. Coefficient of traction is defined by,

$$C_T = \frac{\text{horizontal thrust force}}{\text{weight}} \tag{19}$$

By assuming a linear relationship between horizontal thrust force and the torque applied to the wheel, and knowing that the vehicle weight stays constant, Eq. (18) can be reduced to one relating wheel slip and torque:

$$T = T_{max}\left[1 - \frac{B}{s}(1 - e^{-\frac{s}{B}})\right] \tag{20}$$

where T is torque and T_{max} is the maximum torque sustainable by the soil.

3.2. *Experimental Validation*

Experimental trials were performed to confirm that the torque/slip relationship could be modeled using Eq. (20). The vehicle was run (in the field) over a number of different paths, with different soil conditions, and all sensor data (including torque measures) were logged against time. For these trials, the vehicle navigation system as outlined in Section 2.4 with the laser scanner included in the EKF was used.

The recorded sensor data was post-processed to determine the slip during each time step, using Eq. (1). The actual left and right wheel speeds, v_{al}, v_{ar} were approximated using the Euclidean distance traveled by the wheel in time τ between time steps k, $k+1$ computed from the vehicle state vector estimated by the EKF incorporating the laser scanner observations. The measured wheel speeds were taken from the odometric counts:

$$v_m = \frac{\Gamma R_w}{\tau} z_{odo}$$

It is assumed that the length of the arc of the wheel's actual path and the Euclidean distance between the wheel position at time steps k and $k+1$ are approximately the same; this is reasonable for a sufficiently small time step, and low path curvatures. It is also assumed that, although the odometric data is used by the EKF in computing vehicle position, the presence of the high-accuracy laser scanner observations minimises the influence of slip on the position estimates themselves.

From the definition of slip (Eq. (1)) it can be seen that when the vehicle is at low speeds or stationary, both measured and actual speeds are small, and the term $\frac{v_a}{v_m}$ is ill conditioned. We therefore consider initially straight travel and eliminate data with near-zero speed. Figure 2 illustrates the observed torque/slip relationship. Note that the units of T and T_{max} are unimportant since the model parameters will be estimated on-line, and thus scale of the torque axis can be arbitrary.

The data is quite noisy, as indeed is that of Okello et al., but shows a clear trend in the torque/slip

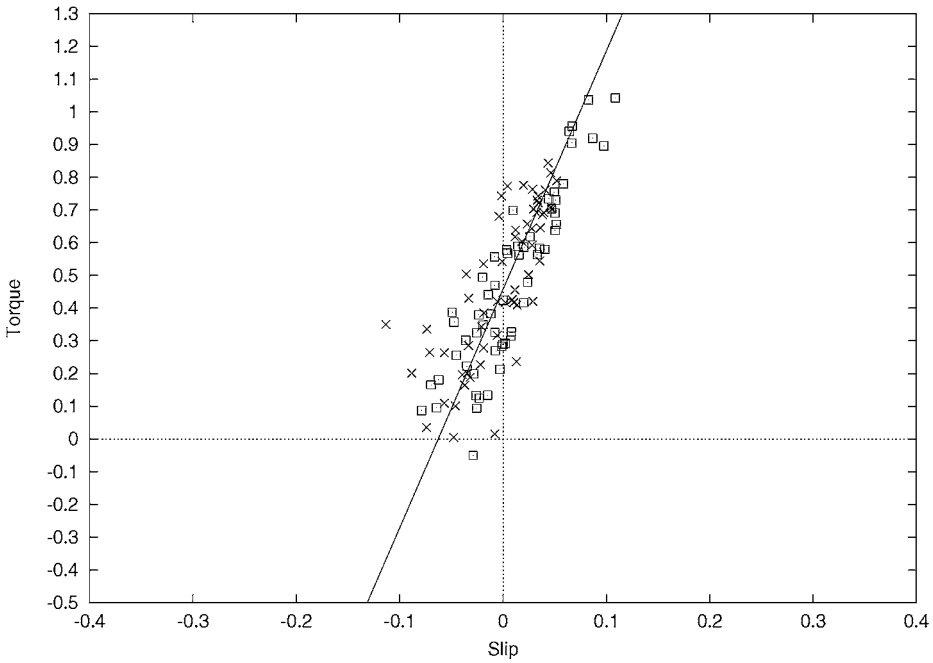

Figure 2. Measured torque against slip for straight line motion: ⊡—left wheel, ×—right wheel. Solid line shows best linear fit to the data points.

relationship. For the data shown the relationship between torque and slip appears to be near linear, and a unique curve of the form given in Eq. (20) cannot reliably be fitted. This suggests that, for the values of slip being experienced by the vehicle, only the part of the torque/slip relationship close to the origin is observed, and that a linear approximation is sufficient.

It was expected that the data would fit a model that passes through the origin; visually this does not appear to be the case. This is confirmed by the best fit line shown in Fig. 2, which has form $T = 0.4575 + 7.2874s$. This is best explained by error in the measured wheel diameter which is used to calculate the values of slip; any errors in the actual diameter will cause the best fit line representing the data to be moved away from the origin.

Assuming that slip remains small and expanding the model, using Taylor's series, about zero:

$$T = T_{max}\left[1 - \frac{B}{s}(1 - e^{-\frac{s}{B}})\right] \tag{21}$$

$$= T_{max}\left[1 - \frac{B}{s}\left(1 - \left(1 - \frac{s}{B} + \frac{s^2}{2B^2} - \frac{s^3}{6B^3} + \cdots\right)\right)\right] \tag{22}$$

$$= \frac{T_{max}}{2B}\left(s - \frac{s^2}{3B} + \cdots\right) \tag{23}$$

Discarding second and higher order terms, the model reduces to the linear form,

$$T = k_s s \tag{24}$$

where $k_s = \frac{T_{max}}{2B}$. This line must go through the origin since the wheel can experience no slip if it is experiencing no torque. To determine the effect of error in wheel radius on measured slip s_m, let s_a be the actual slip, where $s_m \neq s_a$ because measured wheel radius $R_m \neq R_a$, the actual rolling radius. So,

$$s_m = 1 - \frac{v_a}{\omega R_m} \tag{25}$$

$$s_a = 1 - \frac{v_a}{\omega R_a} \tag{26}$$

Subtracting Eq. (25) from Eq. (26) gives

$$s_a - s_m = \frac{v_a}{\omega}\left[\frac{1}{R_m} - \frac{1}{R_a}\right] \tag{27}$$

But, from Eq. (26),

$$\frac{v_a}{\omega} = (1 - s_a)R_a \tag{28}$$

and substituting this into Eq. (27) gives

$$s_a - s_m = (1 - s_a)\left[\frac{R_a}{R_m} - 1\right] \tag{29}$$

and so,

$$s_a = s_m\left(\frac{R_m}{R_a}\right) + \left(1 - \frac{R_m}{R_a}\right) \tag{30}$$

So, if the model is $T = k_s s_a$, then the plots of T against s_m should take the form

$$T = k_s\frac{R_m}{R_a}s_m + k_s\left[1 - \frac{R_m}{R_a}\right] \tag{31}$$

It can be noted from this that the function is still linear, though not through the origin, as shown by the experimental data.

The shape of the wheel when in contact with the ground is a function of tire inflation pressure, tire wall strength and the maximum pressure that the ground can support. If the tire is resting on solid ground, the ground will not be deformed, but part of the tire will be flattened. If the ground is soft, the tire will remain round like a rigid wheel and the tire will sink into the soil. On grounds in between these, a normal tire will be flattened a little, but will also experience some sinkage.

To find the effective wheel radius of the vehicle, the vehicle was towed with the transmission disconnected from the wheels so that they were allowed to rotate freely. Readings from the odometric system allowed the rotation of the wheels to be accurately calculated. The actual distance travelled by each wheel along the ground was carefully measured and from this the effective wheel radius could be calculated. This procedure was undertaken both on soil and on concrete. On soil the wheel radii were found to be 0.283 m, 0.287 m for the left and right wheels respectively; on concrete however, the radii were 0.275 m for both wheels. These measurements confirm that the effective radius is a function of the surface.

4. Kalman Filter Odometric Observation Model

It was shown that the relationship between torque and slip was linear but did not pass through the origin,

instead having a non-zero intercept due to the effects of errors in wheel radius.

While it would be possible to use a model with intercept and gradient parameters, a model with wheel radius and gradient parameters was adopted as it was felt that the wheel radius had more obvious a physical meaning than the intercept of the torque-slip graph. When deriving the covariance evolution for this parameter, it is simpler to visualize the effects of errors in radius than the effects of errors in the torque-slip graph intercept.

Extra states were added to the state vector to reflect the increase in order of the model. These new state variables were the wheel radius R_w and gradient k for each wheel. Recalling the linear torque/slip model:

$$\begin{aligned} T &= k_s s \\ &= k_s\left(1 - \frac{v_a}{v_m}\right) \end{aligned} \tag{32}$$

where

$$v_a = v \pm \frac{W}{2}\Omega \tag{33}$$

Denoting the angular speed of the wheel by ω_m,

$$v_m = R_w \omega_m \tag{34}$$

where R_w is the radius of the wheel.

Substituting this into Eq. (32) leads to

$$T = k_s - k_s \frac{v \pm \frac{W}{2}\Omega}{R_w \omega_m} \tag{35}$$

but the odometric measurement (number of odometer counts in time τ) can be expressed

$$z_{odo} = \frac{\tau}{\Gamma}\omega_m \tag{36}$$

where Γ is the scaling factor between odometer counts and wheel angular speed.

Substituting for ω_m in Eq. (35) gives

$$z_{odo} = \frac{\tau}{\Gamma}\left[\frac{\left(v \pm \frac{W}{2}\Omega\right)k_s}{R_w(k_s - T)}\right] \tag{37}$$

which forms the new observation model for the odometers with gradient and radius parameters. In order to incorporate the new measurement model into the EKF, the model is differentiated with respect to the state vector; the results of the differentiation are as follows.

$$\frac{\partial z_{odo}}{\partial v} = \frac{\tau k_s}{\Gamma} \times \frac{1}{R_w(k_s - T)} \tag{38}$$

$$\frac{\partial z_{odo}}{\partial \Omega} = \pm\frac{\tau k_s W}{2\Gamma} \times \frac{1}{R_w(k_s - T)} \tag{39}$$

$$\frac{\partial z_{odo}}{\partial R_w} = -\frac{1}{R_w^2} \times \frac{\tau}{\Gamma}\left[\frac{\left(v \pm \frac{W}{2}\Omega\right)k_s}{k_s - T}\right] \tag{40}$$

$$\frac{\partial z_{odo}}{\partial k_s} = -\frac{\tau T}{R_w \Gamma} \times \left[\frac{\left(v \pm \frac{W}{2}\Omega\right)}{(k_s - T)^2}\right] \tag{41}$$

The states k_s and R_w have both been shown to depend upon soil properties, which may be assumed to be locally consistent, but slowly spatially varying. Hence, these parameters must be allowed to evolve; this is achieved by increasing their corresponding variances in the process model (Eq. (7)) in proportion to the distance travelled during the prediction interval.

5. Results

The EKF outlined in the previous section formed one part of the testing. In order to compare the improvement gained through use of the new model, the raw sensor data acquired during the execution of a path by the vehicle was recorded. The data could then be run through four different EKF schemes:

1. The first EKF used only the laser scanner and inertial measurements to update the Kalman filter state variables. These sensors are unaffected by slipping of the wheels, and so this scheme is used as an indication of ground truth.
2. The second EKF used odometric measurements only, neglecting effects of slip. This was included to illustrate the magnitude of cumulative errors affecting odometric positioning.
3. The third EKF used all available sensor updates, but did not include a slip model. In this case, the errors in the dead reckoning would cause errors in the estimate in position due to the confidence placed in them.
4. The final EKF incorporated the slip model which was derived in the previous section.

The EKFs were implemented off-line as a reconstruction of the actual vehicle EKF so that sensor data

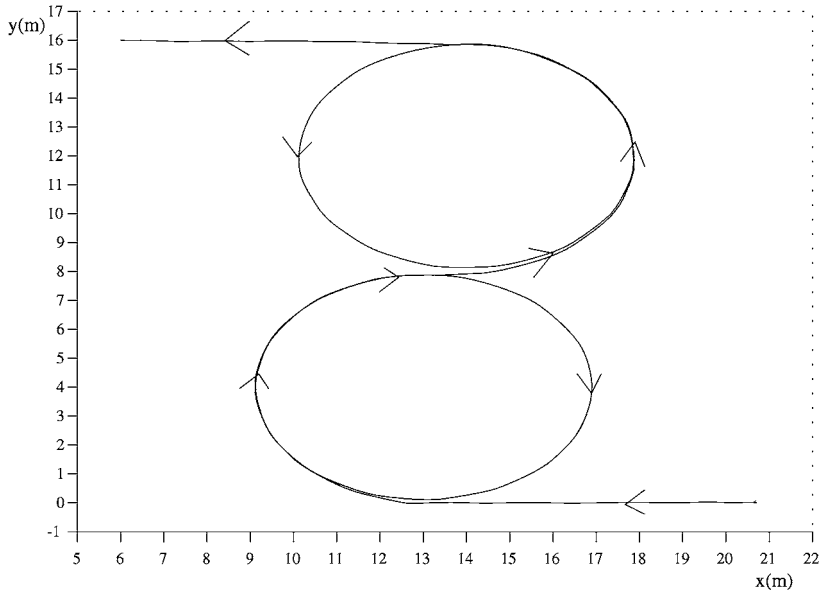

Figure 3. Plot of large radius vehicle path used for model performance comparison.

collected in a single experimental run could be utilized in each case. The outputs of all the EKFs can thus be compared to show the effects of the different schemes.

To determine whether the torque-slip model adequately represented the actual torque-slip relationship, a vehicle path was chosen such that there would be little change in model parameters over the path. The path seen in Fig. 3 was used, which consists of one and a half loops in first a clockwise, then an anticlockwise direction, each of 4 m radius. To allow the slip model parameters to converge to steady values, only the portion of the path where the vehicle was circling clockwise at constant speed is considered here.

Figure 4(a) shows the vehicle path as generated by the EKF Scheme 1 above. This is taken to be the true path. Any deviation from this path that is apparent when the other EKF schemes are used may be attributed to errors in odometric interpretation.

Figure 4(b) shows the path computed using odometric dead reckoning alone with no consideration of slip, as generated by EKF Scheme 2 above. This path that diverges significantly from the actual path given by scheme 1. This is clearly unsuitable for accurate vehicle navigation, but is presented as an indication of the errors present in odomeric data.

Figure 4(c) shows the reconstruction of the vehicle path when the EKF had all sensor updates available, but no slip model, as outlined by EKF Scheme 3 above. The addition of the other sensors can be seen to improve the navigation greatly, but the unconsidered errors in dead-reckoning due to slip, cause the path not to be identical to the true path (Fig. 4(a)). Note that this Scheme 3 was used for vehicle control when the sensor data was collected and hence appears closest to the *commanded* path in Fig. 3, though this does not indicate that it is an accurate representation of the *actual* path taken.

Figure 4(d) shows the reconstruction of the vehicle path using the slip model, outlined by EKF Scheme 4 above. This path appears visually a little closer in form to the actual path.

In attempt to quantify the advantage gained by using the slip model, a value of error at each time step was obtained. This error value was the deviation between the actual vehicle position as given by the laser and gyro only EKF output (EKF Scheme 1), and the position as estimated by the EKFs incorporating odometric observations with and without the slip model (EKF Schemes 3 and 4).

Figure 5(a) shows a plot of the deviation for each time step for the path generated by the EKF using full sensor data but no slip model. It appears that the deviation is not entirely independent of time or vehicle position along the path.

Figure 5(b) shows a plot of the deviation for each time step for the path generated by the EKF

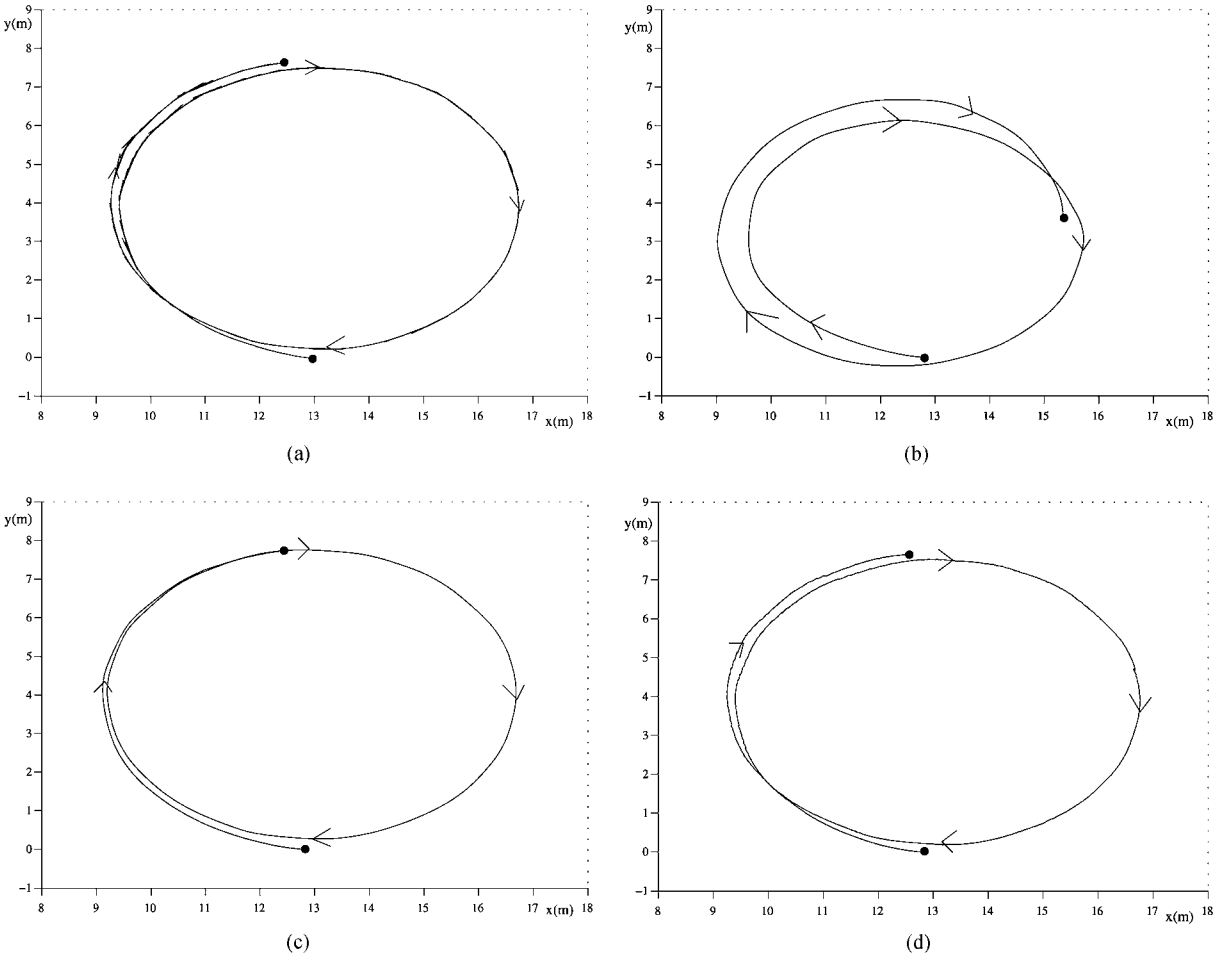

Figure 4. Plot of vehicle path generated by EKFs using: (a) laser and gyro only; (b) dead reckoning only; (c) all sensor data, slip unmodeled; (d) all sensor data and two parameter slip model.

incorporating the slip model. It can be seen that the deviation does not vary in the same systematic way. This would suggest that there is no time or position dependent factor that is not reflected in the slip model.

The mean deviation was calculated and is given in Table 1. This value can be thought of as a numerical measure of the performance of the EKF over this path. The two parameter slip model EKF gives a mean deviation that is approximately half that of the full sensor EKF without the slip model. This shows that the EKF performs better with the slip model included than without, and confirms that the model better represents the odometric observations.

In order to assess the performance of the model mathematically, the innovations of the slip aware dead reckoning update stage were considered. Tests for Kalman filter consistency are outlined by Bar-Shalom and Fortmann (1988); their criteria for consistency of an EKF are:

1. The state errors should be zero-mean (unbiased) and compatible with their covariance, as yielded by the filter.
2. The innovations should have the same property.
3. The innovations should be white (uncorrelated in time).

The first criterion cannot be tested in real data applications as the true state is not available except in simulations. The last two criteria are consequences of the first, and are more readily tested.

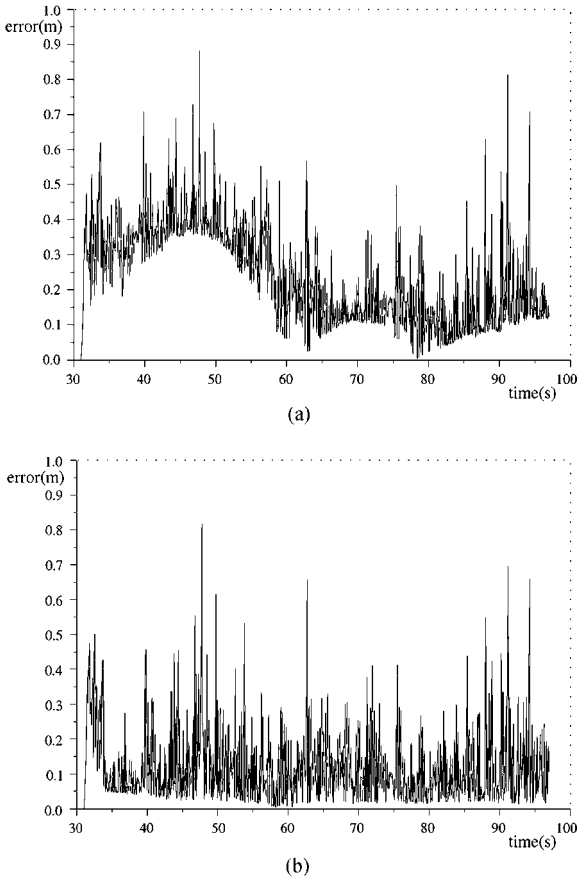

Figure 5. Plot of deviation against time for each time step: (a) with all sensor data, slip unmodeled; (b) with all sensor data and two parameter slip model.

Whiteness of the innovations can be tested using the autocorrelation statistic

$$\bar{\rho}(l) = \sum_{k=1}^{K} \boldsymbol{\nu}'(k)\boldsymbol{\nu}(k+l) \left[\sum_{k=1}^{K} \boldsymbol{\nu}'(k)\boldsymbol{\nu}(k) \times \sum_{k=1}^{K} \boldsymbol{\nu}'(k+l)\boldsymbol{\nu}(k+l) \right]^{-\frac{1}{2}} \tag{42}$$

which, for $l > 0$, should be approximately normally distributed with variance $1/K$ if the innovations are zero-mean and white.

Table 1. Mean error values for the two EKF schemes.

EKF scheme	Mean deviation (m)
3. All sensors, slip unmodeled	0.243
4. All sensors, slip modeled	0.127

The output of the autocorrelation statistic can be seen in Fig. 6(a) and (b), which show the output with slip unmodeled, and with the slip model model respectively. The 95% confidence interval is also shown, i.e., $\pm 1.96/\sqrt{K}$, where in this case $K = 1099$.

It can be seen from the first of these two that the innovations without the slip model are clearly not zero-mean. There also appears to be a periodic element to the autocorrelation statistic. All of the points lie outside the confidence interval.

In the second plot, showing the result for the dual parameter model the autocorrelation values appear in general much closer to zero, with no apparent periodic components. In this case 97.09% of the points lie within the confidence interval. The means and variances of the autocorrelation statistic both with and without the slip model can be seen in Table 2.

It can be seen that the mean with slip modeled is much closer to zero than that without, and the variance is also smaller. This confirms that the slip-aware model better represents odometric data.

The compatibility of the innovations with their variance (criterion 2) can be tested with the statistic

$$\bar{\epsilon}_\nu = \frac{1}{K} \sum_{k=1}^{K} \boldsymbol{\nu}'(k)\mathbf{S}^{-1}(k)\boldsymbol{\nu}(k) \tag{43}$$

which is the time-averaged normalised innovations squared. For white, zero-mean innovations with covariance $\mathbf{S}(k)$, then $K\bar{\epsilon}_\nu$ has a chi-square distribution with Kn_z degrees of freedom, where n_z is the dimension of the measurement. A confidence region can be determined for a selected the level of significance; for large values of Kn_z, the chi-squared values may be approximated by:

$$\chi^2_n(\alpha) \approx n \left[1 - \frac{2}{9n} + u_\alpha \sqrt{\frac{2}{9n}} \right]^3 \tag{44}$$

where n is the number of degrees of freedom and u_α is such that $\Pr(G > u_\alpha) = \alpha$, and $G \sim N(0, 1)$.

The time-averaged normalised innovations squared statistic (Eq. (43)) was applied to the two EKF innovation sets. The number of samples K was 1099, and the measurement had dimension n_z of 2. For a significance of 0.05 and $n = Kn_z = 2198$, the confidence region for $\bar{\epsilon}_\nu$ obtained using Eq. (44) has lower bound 1.8831 and upper bound 2.1204.

The values of $\bar{\epsilon}_\nu$ obtained from the innovation sequence using Eq. (43) are given in Table 3.

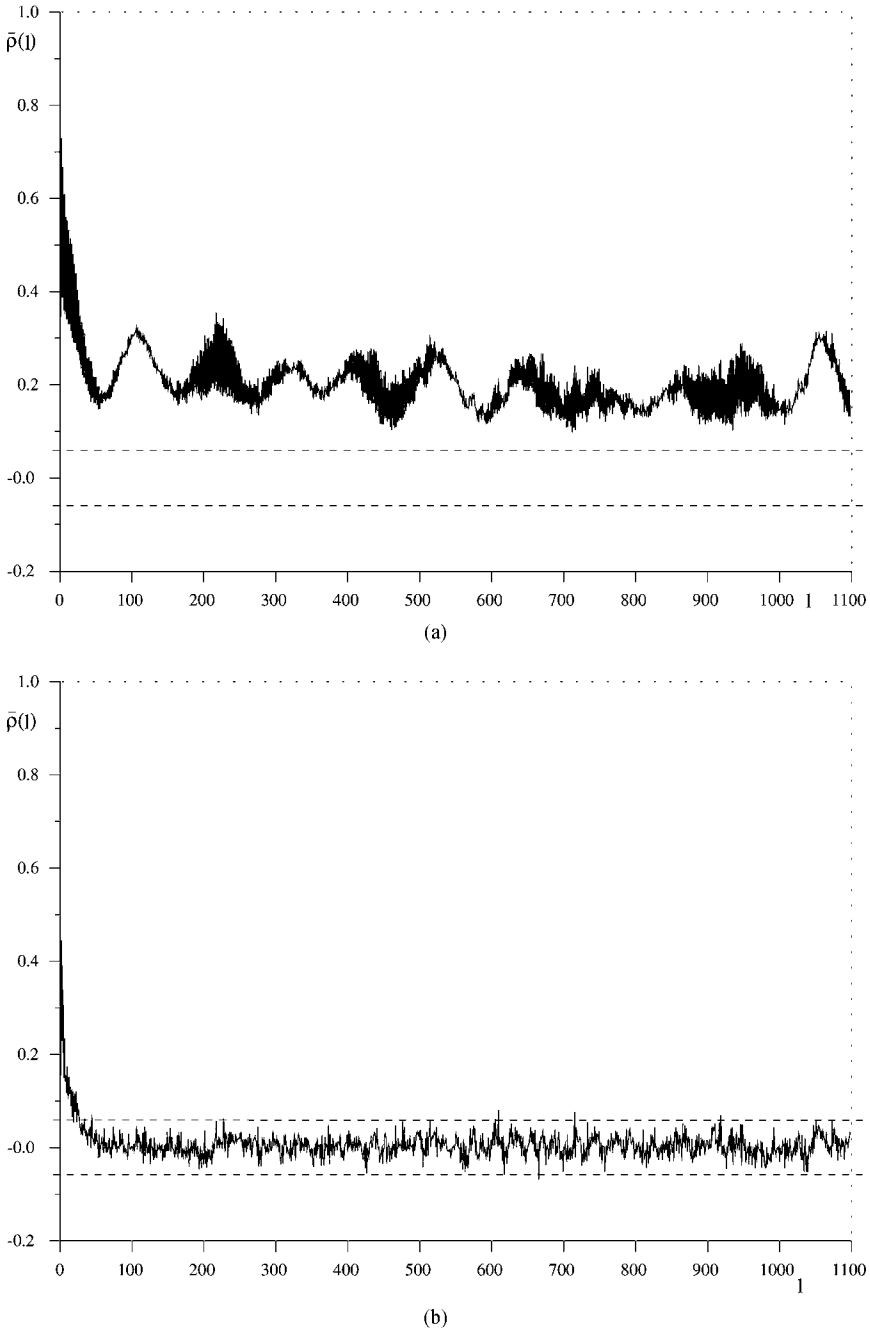

Figure 6. Plot of the autocorrelation statistic for the dead reckoning innovations; (a): slip unmodeled, (b): slip modeled.

Although neither of these fall within the confidence region, the result from the EKF with slip-aware model is somewhat closer than that without. It is likely that the underestimation of innovation variance $\mathbf{S}$ is a contributing factor to the larger than expected values of $\bar{\epsilon}_\nu$; this is a well known weakness of the EKF, arising from neglecting of higher order terms in the variance propagation calculation.

As a practical test of the new odometric model in a situation relating more closely to an agricultural scenario, a path was constructed which consists of straight line travel, with alternate right and left 180° turns.

Table 2. Table of means and variances for the autocorrelation statistic of innovations with and without slip model.

Model	Mean	Variance
Slip unmodeled	0.2068	0.0678
Slip modeled	0.0081	0.0444

Table 3. Table of the time-averaged normalized innovations squared statistic for EKF Schemes 3 and 4.

Model	$\bar{\epsilon}_\nu$
Slip unmodeled	5.1860
Slip modeled	3.1836

Again the 'ground truth' path was computed using laser scanner and inertial sensors only, i.e., Scheme 1 above.

Against this baseline, paths were computed using a sensor combination of the laser scanner and odometers only. The results are shown in Fig. 7. To simulate loss of external position data, the laser scanner observations were ignored after a point 50 s in to the path (marked by a cross in the figure). This trial was performed using the the original odometric model where slip is neglected (seen in Fig. 7(a)), and the new slip-aware odometric model (Fig. 7(b)). In the original model a carefully measured effective wheel radius was used. It can be seen that when slip is neglected, odometric measures indicate that the outer wheel during the second turn has traveled further than it has in reality, leading to an orientation error of around 10° on exit from the turn, resulting in a final position error of 1.97 m.

In the second trial, where the slip is modeled, the first part of the path serves to allow the state variables for effective wheel radii, and torque/slip relationship to be observed. In the subsequent turn, the accuracy of odometric interpretation is improved by an order of magnitude; the final position error is 0.21 m.

6. Conclusions

We have considered the suitability of traction models for off-road vehicles, derived from soil mechanics and agricultural engineering literature, as a basis for a slip-aware odometric model for off-road autonomous vehicle navigation.

Using wheel torque and slip measurements from an experimental vehicle, it has been verified that the observed relationship between torque and slip fits the classical model reported in the literature, but that for our low draught force application, the slip experienced remains small enough that the relationship can be adequately modeled as linear. The constant of proportionality is a function of soil properties which may be spatially variable, and so must be estimated.

Measurements of effective wheel rolling radius have confirmed that its value depends upon soil properties, hence wheel radius must also be estimated.

A simple two parameter model where the wheel rolling radius and the gradient of a linear torque/slip relationship are included as states to be estimated in an extended Kalman filter has been implemented and tested using sensor data from the experimental vehicle; comparisons showed that the new odometric model

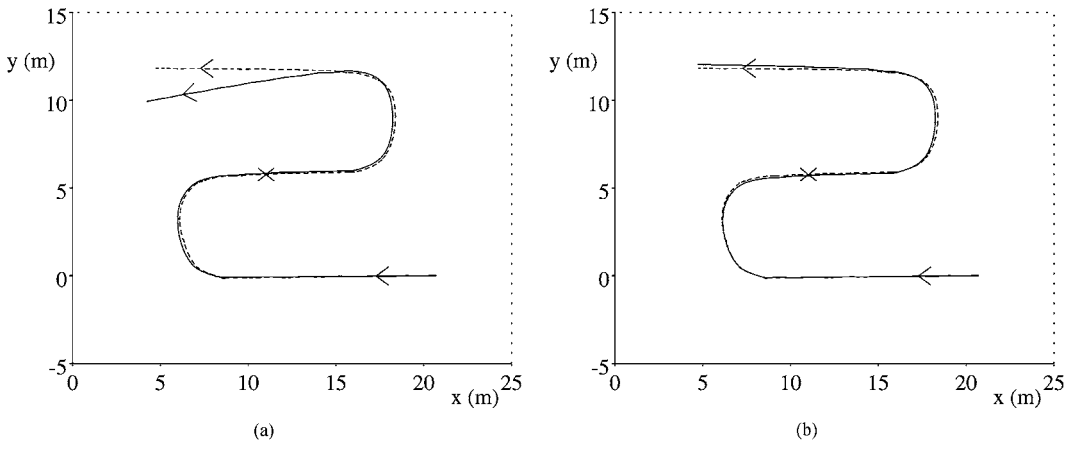

Figure 7. Comparison of odometric models: (a) original, slip neglected; (b) new, slip modeled.

improved filter consistency and position estimation accuracy.

Acknowledgment

This work was supported by the Biotechnology and Biological Sciences Research Council.

References

Bar Shalom, Y. and Fortmann, T. 1988. *Tracking and Data Association*, Academic Press: New York.

Bekker, M.G. 1960. *Off-The-Road Locomotion*, University of Michigan Press.

Bekker, M.G. 1962. *Theory of Land Locomotion*, University of Michigan Press.

Borenstein, J. 1996. Measurement and correction of systematic odometry errors in mobile robots. *IEEE Trans. Robotics and Automation*, 12(6):869–880.

Craig, R.F. 1992. *Soil Mechanics*, 5th edn., Chapman and Hall.

Hague, T., Marchant, J.A., and Tillett. N.D. 1997. Autonomous robot navigation for precision horticulture. In *IEEE Int. Conf. Robotics and Automation*, Albuquerque, pp. 1880–1885.

Hague, T. and Tillett. N.D. 1996. Navigation and control of an autonomous horticultural robot. *Mechatronics*, 6(2):165–180.

Jahns. G. 2000. Special issue on navigating agricultural field machinery. *Computers and Electronics in Agriculture*, 25(1/2).

Janosi, Z. and Hanamoto, B. 1961. The analytical determination of drawbar pull as a function of slip for tracked vehicles in deformable soils. In *ISTVS 1st Int. Conf. on Mechanics of Soil-Vehicle Systems*, Edizioni Minerva Tecnica, Torino, Italy, pp. 707–736.

Le, A.T., Rye, D.C., and Durrant Whyte, H.F. 1997. Estimation of track-soil interactions for autonomous tracked vehicles. In *IEEE Int. Conf. Robotics and Automation*, pp. 1388–1393.

Okello, J., Dwyer, M.J., and Cottrell, F.B. 1994. The tractive performance of rubber tracks and a tractor driving wheel tyre as influenced by design parameters. *J. Agric. Eng. Research*, 59(1):33–43.

Scheding, S., Dissanayake, G., Nebot, E., and Durrant Whyte, H. 1997. Slip modeling and aided inertial navigation of an lhd. In *IEEE Int. Conf. Robotics and Automation*, pp. 1904–1909.

Smith, G.N. 1982. *Elements of Soil Mechanics for Civil and Mining Engineers*, 5th edn., Granada Publishing.

Willner, D., Chang, C.B., and Dunn, K.P. 1976. Kalman filter algorithms for a multi-sensor system. In *Proc. IEEE Int. Conf. Decision and Control*, pp. 570–574.

David Lindgren received his M.Eng degree in Engineering Science from Oxford University in 1997. He was awarded his D.Phil degree in 2001 for research conducted jointly between the Oxford University robotics research group and Silsoe Research Institute, part of which is reported here.

Tony Hague received his B.Sc. degree in Computer Systems Engineering from Warwick university in 1988, and a D.Phil from Oxford university in 1993. He currently works at Silsoe Research Institute in the Robotics and Automation group, where his research interests include autonomous vehicle path planning, navigation and vision-based guidance.

Penny Probert Smith is Reader in Engineering Science at the University of Oxford. Her research interests are in sensing and multi-sensor fusion, with particular interests in reasoning under uncertainty.

John Marchant received his B.Sc. degree in Electrical and Electronic Engineering from the City University, London, in 1970 and a Ph.D. from the same university in 1981. After graduating, he spent four years in the aerospace industry before joining what is now Silsoe Research Institute in 1974. He has worked on many aspects of research for agricultural engineering and, since 1986, has been involved in robotics research, especially machine vision aspects. Adjuncts to his professional life include running and banjo playing.